Nanostructured complex oxides as a route towards thermal behavior in artificial spin ice systems

R. V. Chopdekar,[1,*] B. Li,[1] T. A. Wynn,[1] M. S. Lee,[1] Y. Jia,[1] Z. Q. Liu,[2,†] M. D. Biegalski,[2] S. T. Retterer,[2]
A. T. Young,[3] A. Scholl,[3] and Y. Takamura[1]

[1]*Department of Materials Science and Engineering, University of California, Davis, Davis, California 95616, USA*
[2]*Center for Nanophase Materials Sciences, Oak Ridge National Laboratory, Oak Ridge, Tennessee 37831, USA*
[3]*Advanced Light Source, Lawrence Berkeley National Laboratory, Berkeley, California 94720, USA*

We have used soft x-ray photoemission electron microscopy to image the magnetization of single-domain $La_{0.7}Sr_{0.3}MnO_3$ nanoislands arranged in geometrically frustrated configurations such as square ice and kagome ice geometries. Upon thermal randomization, ensembles of nanoislands with strong interisland magnetic coupling relax towards low-energy configurations. Statistical analysis shows that the likelihood of ensembles falling into low-energy configurations depends strongly on the annealing temperature. Annealing to just below the Curie temperature of the ferromagnetic film ($T_C = 338$ K) allows for a much greater probability of achieving low-energy configurations as compared to annealing above the Curie temperature. At this thermally active temperature of 325 K, the ensemble of ferromagnetic nanoislands explore their energy landscape over time and eventually transition to lower energy states as compared to the frozen-in configurations obtained upon cooling from above the Curie temperature. Thus, this materials system allows for a facile method to systematically study thermal evolution of artificial spin ice arrays of nanoislands at temperatures modestly above room temperature.

I. INTRODUCTION

Frustration in magnetic systems occurs due to the inability to find a configuration that simultaneously minimizes all neighboring interactions, and can be found in systems with structural disorder (e.g., spin glasses) or systems with structural order but multiple competing interactions due to the geometry of the ordered state (e.g., pyrochlore structure crystals) [1,2]. There has been considerable interest in the fabrication of two-dimensional analogs of geometrically frustrated systems via an ensemble of nanomagnets to explore the physics of frustrated systems, including the effect of long-range dipolar interactions and the emergence of monopolelike defects [3–7]. The magnetostatic energy barrier for nanomagnet reversal can be considerably higher than room temperature, but effective thermodynamics of such athermal systems have been explored by enumerating the statistical likelihood of vertices with different magnetostatic energies [8,9]. If the nanoislands are thermally active near room temperature, thermally driven phenomena such as magnetic relaxation processes and monopolelike defect propagation can be measured with real-space imaging techniques. Prior magnetic microscopy experiments aimed at examining these effects in metallic nanostructures have achieved success in observing thermally induced low-energy magnetic configurations frozen-in during sample preparation [10]. Subsequent experiments have shown that ultrathin Permalloy nanoislands have a thickness-dependent blocking temperature such that 3-nm-thick islands yield a superparamagnetic blocking temperature near 300 K [11]. Artificial spin ice structures fabricated from ultrathin

Fe layers embedded in Pd have also exhibited thermalization behavior at cryogenic temperatures [12,13].

Experiments with ultrathin metallic nanoislands face challenges due to differences in blocking temperature between nominally identical islands caused by small changes in material thickness, as well as the possibility of rapid oxidation, which can lead to suppression of magnetization on the time scales of experimental measurements. These issues can make it difficult to separate thermodynamic evolution of an artificial spin ice system from magnetization configuration changes due to island-island variation or materials degradation. In lieu of using nearly superparamagnetic islands, thermalization of artificial spin ice arrays in thicker Permalloy islands was clearly demonstrated [14], but these studies required temperatures above 800 K, which introduced possible issues of interdiffusion of the magnetic material with the substrate as well as lateral diffusion of the nanoisland material. Recent studies have shown that $Gd_{0.3}Co_{0.7}$ and $FePd_3$ (bulk Curie temperatures near 500 K) can be used in artificial spin ice geometries to exhibit thermally active behavior after appropriate annealing protocols [15,16]. In contrast, the use of a nanostructured epitaxial complex oxide such as $La_{0.7}Sr_{0.3}MnO_3$ (LSMO) could permit the study of thermally active artificial spin ice geometries just above room temperature due to a bulk Curie temperature of 370 K. Furthermore, LSMO exhibits good chemical stability in both vacuum and standard atmosphere environments up to 873 K [17], permitting a broad range of annealing conditions. We explore thermal demagnetization in ensembles of coupled LSMO nanoislands and show that this artificial spin ice materials system offers a facile route to explore thermal effects in geometrically frustrated artificial systems at temperatures only slightly above room temperature.

II. EXPERIMENTAL METHODS

Epitaxial LSMO films with 40-nm thickness were grown on conducting (001)-oriented $Nb:SrTiO_3$ substrates via pulsed

---

*Present address: Department of Materials Science and Engineering, University of California, Davis, One Shields Ave., Davis, CA 95616, USA; rchopdekar@ucdavis.edu

†Present address: School of Materials Science and Engineering, Beihang University, Beijing 100191, China.

laser deposition. Substrates were held at a deposition temperature of 700 °C in an ambient oxygen pressure of 200–300 mTorr with a laser fluence of 1 J/cm², and a postdeposition anneal in 300 Torr of oxygen minimized the presence of oxygen vacancies. The crystallinity of the films was characterized by high-resolution x-ray diffraction, with reciprocal space maps of the 103 reflection indicating that the films were wholly pseudomorphic. Following the LSMO deposition, ensembles of coupled nanomagnets were defined with a 70-nm-thick chromium hard mask patterned via an electron-beam lithography liftoff technique. A flood implant of 10^{15} Ar⁺ ions/cm² at an energy of 50 keV caused the regions of LSMO not protected by the Cr hard mask to be rendered amorphous and paramagnetic, while the crystalline LSMO protected by the mask retained its ferromagnetic order at room temperature [18,19]. At this dose, the magnetization of the implanted regions is reduced to less than 5% of the as-deposited crystalline LSMO as measured by magnetometry at 10 K. The Cr mask was removed from the sample after the implant and before subsequent measurements. Magnetoresistance measurements of a 500-nm-wide and 20-μm-long LSMO wire patterned using this technique (see Supplemental Material, Fig. S1 [20]) gave a metal-insulator transition temperature of 338 K. This transition temperature is coincident with the Curie temperature due to the double-exchange mechanism in LSMO [21].

The nanoisland shape was chosen to be a stadium geometry (rectangle with semicircles at opposite ends), with total island length fixed at 470 nm while the widths of the islands were varied between 100 and 225 nm. The width variation served to control both the island shape anisotropy and the total magnetic moment m per island, but for all widths the magnetization was Ising-like and aligned along the island's long axis. While micron-scale (001)-oriented LSMO nanostructures have non-negligible magnetocrystalline anisotropy at low temperatures [22], the magnetocrystalline anisotropy constant K_1 linearly decreases with increasing temperature and is close to zero near the Curie temperature [23]. Thus, the nanoscale islands in this work were found to be dominated by shape anisotropy at all measurement temperatures, and experimentally were single domain with the magnetization directed along the island long axis, regardless of crystallographic orientation. The lattice spacing between neighboring kagome or square ice unit cells a was varied between 500 and 640 nm to tune the interisland coupling strength m^2/a^3, which reflects the scale of the dipolar interaction [24]. We treat each nanoisland as an Ising-like macrospin and estimate the dipolar interaction energy of an ensemble of N nanoislands as

$$E_{\text{dipolar}} = \sum_{i<j}^{N} \frac{\mu_r \mu_o}{4\pi r_{ij}^3} [\overline{m_i} \cdot \overline{m_j} - [3/(r_{ij})^2](\overline{m_i} \cdot \overline{r_{ij}})(\overline{m_j} \cdot \overline{r_{ij}})],$$

with m_i as the magnetic moment of the ith nanoisland, r_{ij} as the distance between the ith and jth nanoisland, and $\mu_r \mu_o$ as the permeability of the material between the nanoislands. Unlike previous studies in which air or vacuum separate neighboring nanoislands in artificial spin ice ensembles, the paramagnetic amorphous matrix in which the LSMO islands are embedded has a relative permeability greater than 1. The permeability of a 40-nm-thick LSMO film implanted with the same Ar⁺

ion dose across the entire film surface was measured to be approximately 1.1 μ_0 at room temperature.

The dipolar energy and coupling strength can be related to the material's magnetization $M(T)$ and the island volume V_{island} as $\frac{m^2}{a^3} = M^2(T)\frac{V_{\text{island}}^2}{a^3}$. Thus, for a fixed island volume and spacing, the coupling strength may also be tuned as a function of temperature. At room temperature, the interisland coupling strength can be calculated based on a room-temperature saturation magnetization of 225 emu/cm³ for a continuous LSMO film of similar thickness. Room-temperature coupling strengths based on this saturation magnetization and the above island spacings are quantitatively smaller to those obtained for thin Permalloy and cobalt-based spin ice systems [24], and approach coupling strengths of thermally active ultrathin Permalloy islands [11], showing that the lithographically defined LSMO nanoisland ensembles can also offer insights into the physics underlying thermal interactions in artificial spin ice systems.

Imaging of the magnetization orientation as a function of applied magnetic field and variable temperature was measured with Mn *L*-edge soft x-ray photoemission electron microscopy (X-PEEM) at the Advanced Light Source [25]. While magnetic contrast was measureable at all temperatures below room temperature, magnetization images were taken at a sample temperature of 110 K to minimize any thermal evolution of the magnetization and to maximize the x-ray magnetic circular dichroism (XMCD) contrast. A coil built into the sample holder allowed magnetic field pulses of up to 15 mT to be applied parallel to the in-plane projection of the x-ray incidence direction, with the nanoisland magnetization imaged in remanence after any field pulse sequence. A second sample holder with no magnetic coil was also used during thermal annealing sequences so that any stray magnetic field can be excluded from influencing the nanoisland magnetization configuration. The x rays impinged upon the sample at a 30° grazing angle with respect to the surface and were set to be within 5° of the in-plane [100] crystal direction. The sensitivity axis of the X-PEEM imaging is parallel to the incoming x-ray direction, and is oriented horizontally from the right in the figures below. The white and black contrast indicates magnetization projections pointing to the right and left, respectively, while a gray contrast indicates zero magnetization or a magnetization orthogonal to the sensitivity axis [26]. The nanoisland magnetization direction, confined to be along the long axis of the island due to shape anisotropy, was determined from the projection of the XMCD contrast along the horizontal axis. Magnetic force microscopy (MFM) at room temperature in atmosphere (Supplemental Material [20], Fig. S2) shows domain configurations consistent with those found with X-PEEM imaging, and no evidence of induced magnetization in the implanted matrix between neighboring nanoislands.

III. RESULTS AND DISCUSSION

Two sets of lithographically defined nanoisland ensembles were fabricated in the epitaxial LSMO films: large ensembles of islands arranged in artificial square ice geometries, and smaller ensembles of islands arranged on kagome lattices. The former geometry is comprised of frustrated vertices with
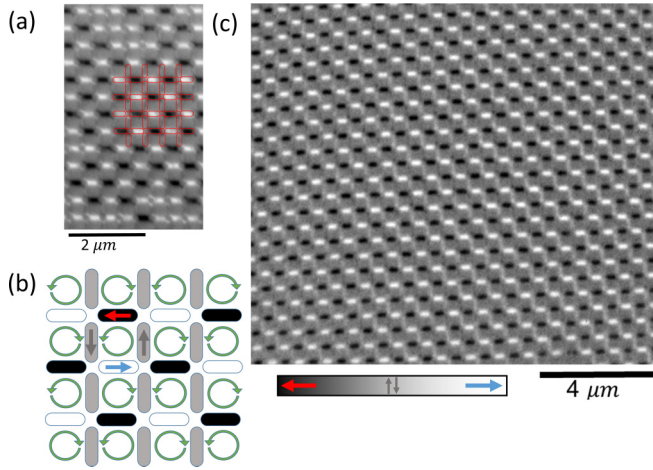
FIG. 1. (a) X-PEEM XMCD image of an artificial square ice array brought to ground state through a magnetic field demagnetization protocol. Epitaxial 470 nm × 175 nm × 40 nm LSMO nanoisland locations are outlined in red. (b) Schematic of ground-state nanoisland magnetization configuration as seen with X-PEEM magnetic sensitivity axis along the horizontal direction parallel to the [100] crystallographic direction, with the red, gray, and blue arrows indicating orientation of the magnetization of the nanoislands. (c) X-PEEM XMCD image of the entire artificial square ice array brought to ground state via 325-K thermal demagnetization protocol.

four islands, while the latter has frustrated vertices of three islands. We directly compared the magnetic configurations of these square and kagome nanoisland ensembles after an alternating magnetic field demagnetization protocol and after a thermal cycling of the sample to the vicinity of its Curie temperature. A comparison of these two methods for an extended LSMO square ice array is shown in Fig. 1. After an *ex situ* saturating magnetic field of 100 mT, which gives a white contrast for all horizontal nanoislands, an oscillating magnetic field was brought from 15 mT to zero and a ground-state region of approximately 5 μm diameter is shown in Fig. 1(a). The X-PEEM magnetic contrast expected from a ground-state configuration is schematically depicted in Fig. 1(b), with nanoislands of alternating contrast along the horizontal direction and negligible contrast along the vertical direction. Due to the slight misorientation between the x-ray incidence direction and the horizontal axis of the square ice array, careful analysis of the vertical nanoisland contrast (Fig. S3) shows a weak alternating contrast which confirms that the center region in Fig. 1(a) is in an antiferromagnetic ground-state configuration, while the regions above and below the outlined islands are still oriented along the saturating field direction. However, further repetitions of the alternating magnetic field protocol could not drive the entire array into a ground-state configuration. On the other hand, thermal cycling of the same sample to 325 K at a rate of 5 K/min using a sample holder with no magnetic coil brought the square ice arrays into a single ground-state configuration across the entire 1200-island arrays [Fig. 1(c)]. Measurements of the weak contrast of the vertically oriented nanoislands confirm that the entire array is in a ground-state configuration (e.g., Fig. S4). Additional square ice ensembles are shown in the Supplemental Material

(Fig. S5), with some isolated high-energy vertices which then can be annealed out after repeated thermal cycling.

While it is clear that the thermal demagnetization protocol can successfully bring square ice arrays into extended ground-state configurations, small ensembles based on the kagome ice geometry can be used to compare the two demagnetizing protocols in a more quantitative manner as a function of increasing number of frustrated vertices contained in the ensemble. One-ring hexagonal ensembles have no frustrated vertices, as each nanoisland only has two nearest neighbors, and the total dipolar energy landscape of the ensemble can be visualized in a straightforward manner due to the small number of islands [24]. For a six-island ensemble, $2^6 = 64$ possible magnetization configurations exist, as each island's magnetization can only orient along its long axis, and the total dipolar energy of the ensemble falls into one of eight degenerate energy levels. As the number of islands in the ensemble increases for two-ring (2^{11} configurations) and three-ring (2^{15} configurations) structures, so too does the magnetic frustration as three-island vertices are now introduced into the ensembles. For the nanomagnet ensembles, the lowest energy magnetic configurations involve vortex or flux-closure patterns which have degeneracy (clockwise or counterclockwise orientation per ring), and higher-energy configurations involve selected islands reversed when compared to this lowest energy state [24].

Figure 2 depicts schematics of one-ring, two-ring, and three-ring nanoisland ensembles and illustrates the occupancy of these ensembles after heating the sample to 350 K (i.e., above their Curie temperature) on a nonmagnetic sample holder and then cooling back to the measurement temperature of 110 K at a rate of approximately 5 K/min. After the anneal, X-PEEM XMCD images were acquired for 12 sets of 100 one-, two- and three-ring ensembles with room-temperature coupling strength m^2/a^3 ranging between 6×10^{-13} and 3×10^{-12} A^{2}m. From the X-PEEM images, the dipolar energy of each ensemble was calculated based on the magnetization orientation of all islands in the ensemble. The ensemble configurations were categorized in order of increasing dipolar energy. The energy landscapes are shown in the Supplemental Material (Figs. S6–S8), and they have close-lying bands of levels separated by energy gaps. The data has been binned into groups of energy levels for the two-ring and three-ring ensembles due to the large number of possible states compared to the number of ensembles measured. For comparison, data for the one-ring ensembles before the annealing protocol is shown in the Supplemental Material (Fig. S9). Error bars are calculated from the square root of the number of observations. In the limit of no coupling between adjacent islands, e.g., with $\frac{m^2}{a^3} \approx 6 \times 10^{-13}$ A^2 m, the degeneracy of the magnetization configurations determines the likelihood of an ensemble being in a specific configuration. On the other hand, with strong coupling between neighboring islands, e.g., $\frac{m^2}{a^3} \approx 3 \times 10^{-12}$ A^2 m, the ensembles are expected to fall into flux-closure magnetization configurations with a high probability.

Annealing above the Curie temperature allows us to probe the effect that these frustrated vertices have on the probability of the ensembles being in a low-energy state. In the regime of high-coupling strength, the one-ring nanoisland ensembles can effectively be brought into the lowest energy configurations with nearly 100% probability, but the lowest energy occupancy
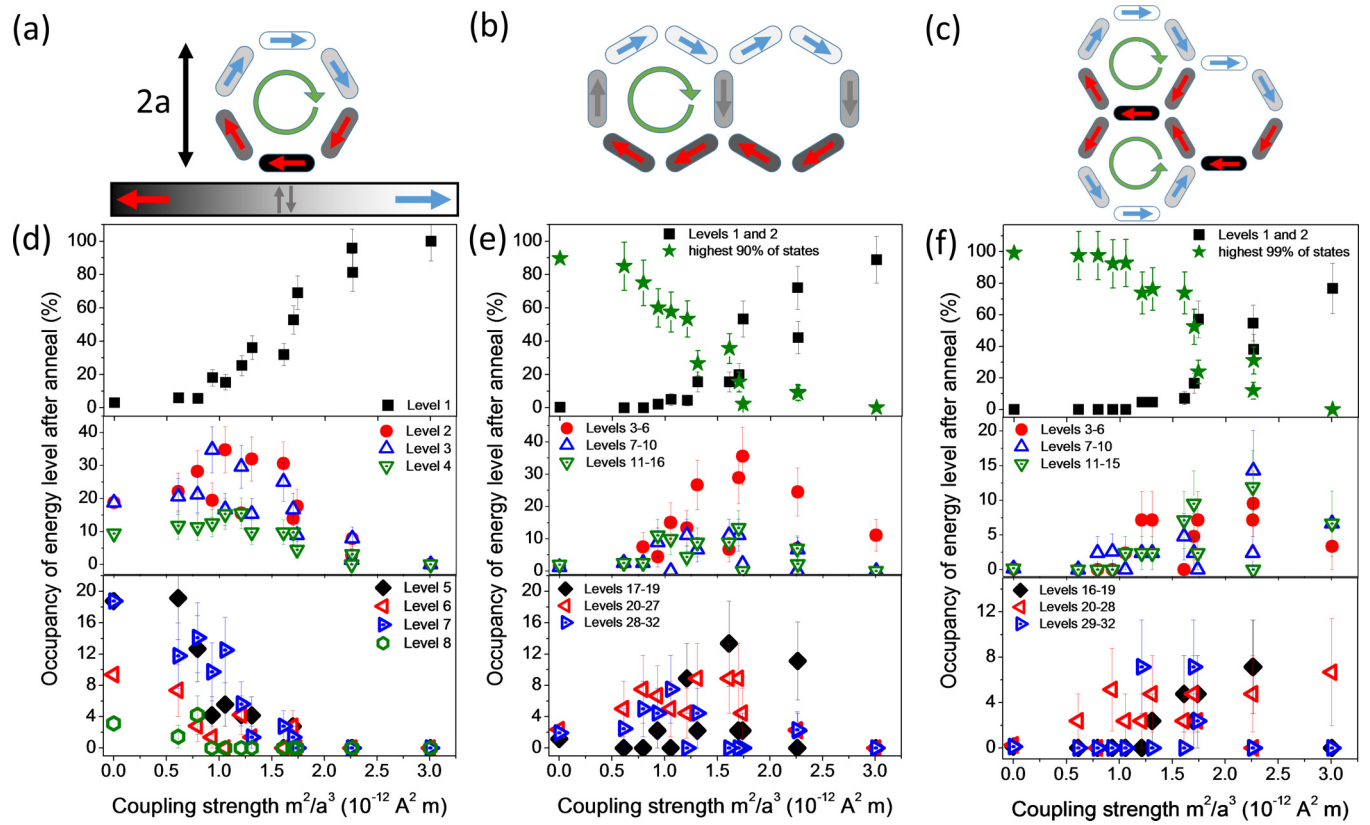
FIG. 2. Schematics of nanoisland magnetization orientation as in Fig. 1(b) for (a) one-ring, (b) two-ring, and (c) three-ring nanoisland ensembles, with *2a* as the ring diameter. Comparison of the occupancy of low-energy magnetization configurations for (d) one-ring, (e) two-ring, and (f) three-ring nanoisland ensembles after a 350-K anneal as a function of dipolar coupling strength. The points at zero coupling strength are calculated from the occupancy of energy levels based on the degeneracy of possible random magnetic configurations.

is noticeably lower in the two-ring (90%) and three-ring (80%) ensembles. These occupancy levels can be tuned between a nearly random magnetization configuration frequency distribution and having all nanomagnet ensembles fall into the lowest energy level for the one-ring ensembles through the choice of lattice spacings between 500 and 600 nm and island widths of 100 and 175 nm. As LSMO is cooled through its Curie temperature, the low-saturation magnetization results in a weak dipolar interaction between neighboring islands for all ensembles. Assuming that thermally driven transitions between energy levels follow a Boltzmann-like distribution, there is a low energy cost of reversing the magnetization of a single island in the limit of weak dipolar interaction. Such thermally active island reversals can lead to nanomagnet ensembles jumping from a ground-state configuration into a higher-energy configuration and vice versa. Thus, these thermally active ferromagnetic ensembles can navigate large regions of their energy landscape in a similar manner to thermally active Permalloy nanoisland ensembles [11]. The above-Curie-temperature thermal cycling protocol and 5-K/min cooling allows many ensembles with intermediate room-temperature dipolar coupling strengths of $1 - 2 \times 10^{-12}$ A^2 m to be frozen into energy configurations slightly higher than the ground state (e.g., levels 2–4 for the one-ring, levels 3–6 for the two- and three-ring ensembles). The occupancy of these particular states has a maximum in the intermediate coupling regime, but as the coupling strength decreases, the occupancy converges to the

values determined by the degeneracy of the configurations as shown for the data points at the $\frac{m^2}{a^3} = 0$ value.

A more carefully designed annealing protocol can increase the overall probability that the ensembles transition to low energy levels by limiting the area of the energy landscape that the ensembles can traverse. While Fig. 2 shows the effect of a single annealing protocol on ensembles of different coupling strengths, Fig. 3 plots the occupation of energy levels for one- and two-ring ensembles at a room-temperature coupling strength of 1.8×10^{-12} A^2 m. Data for three-ring ensembles can be found in the Supplemental Material (Fig. S10) [20]. The ensembles were imaged after an ac magnetic field demagnetization protocol, and subsequently the sample was heated to 325 K for 5 min. At this temperature, the sample was near but below the Curie temperature and the film saturation magnetization is approximately 100 emu/cm^3. A significant number of the ensembles fell into low-energy states after this anneal, higher than the trend seen in Fig. 2. A repeat of this anneal pushed the number of low-energy configurations to even greater occupancy. An *ex situ* anneal in air to 473 K, well above the Curie temperature, returned the sample to similar energy level probabilities as the 350-K anneal data presented in Fig. 2, illustrating that these nanoisland ensembles have a higher percentage of low-energy configurations when held near but below their Curie temperature. A similar thermally active region was probed with a spatially averaged magneto-optical Kerr effect for δ-doped Fe:Pd, with the
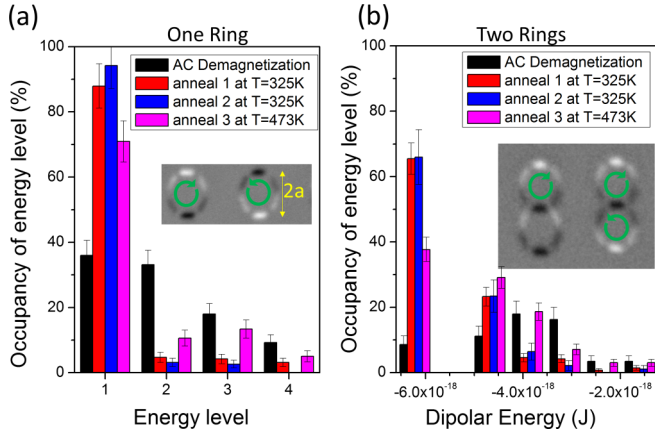
FIG. 3. Effect of demagnetizing protocol on occupancy of low-energy magnetization configurations for (a) one-ring and (b) two-ring ensembles, with the width of each ring of $2a = 1\,\mu$m and a coupling strength of 1.8×10^{-12} A^{2}m. The configurations are binned by calculating the overall dipolar energy of each ensemble, with X-PEEM images of two low-dipolar-energy configurations shown as insets and green arrows showing magnetization direction of rings in flux-closure arrangements.

thermally active region within 25 K of its Curie temperature of 230 K [12].

To evaluate the ability of an annealing protocol to bring the LSMO nanoisland ensembles into a truly thermal state, we took the observed occupancy levels above the ground-state level and examined the relative probability of these excited levels as a function of dipolar coupling strength. Demagnetization protocols for Permalloy-based artificial spin ice arrays have been parameterized by assuming that the population of isolated high-energy vertices in a thermalized array follow a Boltzmann-like distribution [8,14]. The probability of finding an excited vertex in the ith energy level can be described by $P_i(T) = q_i \exp(-\frac{E_i}{k_B T})/Z$, with the ith energy level having an energy E_i and multiplicity of configurations q_i, and Z as the partition function. We apply a similar description to the ring-based nanoisland ensemble energy levels, with the relative occupancy of the excited ith state compared to the lowest energy state, which can be written as $P_i/P_1 = \frac{q_i}{q_1}\exp(-\frac{\Delta E}{k_B T})$.

The datasets from Fig. 2 were appropriately scaled by the multiplicity, and when plotted as a function of the coupling strength (see Supplemental Material, Fig. S11 [20]), all three types of nanoisland ensembles give an effective annealing temperature of 339 ± 2 K. This temperature corresponds to the experimentally observed Curie temperature of the LSMO nanowire within the error of the fitting. Thus, thermal annealing of LSMO nanoisland ensembles at 350 K, above the Curie temperature, can bring these nanoisland ensembles to Boltzmann-like thermalized distributions of energy levels.

As we can prepare the nanoisland ensembles into truly thermalized states through annealing above the Curie temperature, we now directly show real-space measurements of the thermal evolution of a single three-ring ensemble in Fig. 4 as it explores low-lying regions of its energy landscape with annealing below the Curie temperature. We followed the same annealing protocol as described for Fig. 3. While the perimeter of the three-ring structure falls into a head-to-tail flux-closure configuration upon annealing the sample to 325 K [Fig. 4(b)], there still exists a significant degree of freedom in the possible magnetization orientations of the three islands at the center of the ensemble, as seen by the repeated annealing at 325 K [Fig. 4(c)]. The ensemble has no change in overall dipolar energy between the two 325-K anneals, but a reconfiguration of the center islands can occur while the perimeter islands remain in a fixed configuration. In other words, for annealing steps below the Curie temperature, the ensemble is thermally active and can escape local minima of the energy landscape in order to explore other configurations with close-lying energy levels. It is only after an anneal well above the Curie temperature that the entire ensemble can traverse its energy landscape in a more global manner such that a majority of the perimeter island orientations can be reversed.

IV. CONCLUSIONS

In conclusion, complex oxide-based artificial spin ice geometries can be used to explore thermally active behavior of magnetization configurations in a similar manner as metallic systems. The chemical stability and epitaxial nature of these materials minimizes experimental issues such as thickness-dependent island-to-island variations and oxidation-
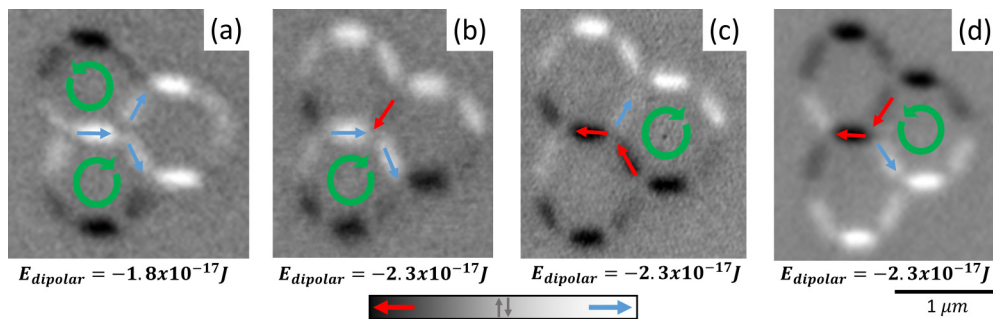

FIG. 4. X-PEEM images of a three-ring frustrated nanomagnet ensemble (a) after an *in situ* ac magnetic field demagnetization at room temperature, (b) after an *in situ* 5-min anneal at 325 K, (c) after another *in situ* 5-min anneal at 325 K, and (d) after a 2-h *ex situ* anneal in air at 473 K. The green arrows indicate the sense of rotation for island groups that are in a low-energy vortex configuration, and the red and blue arrows indicate the direction of magnetization for the center frustrated three-island vertex.

induced changes in island magnetization behavior. The magnetization configuration of the nanoisland ensembles follow a Boltzmann-like distribution upon annealing the sample through its Curie temperature of 338 K. Additionally, these nanoislands are thermally active at temperatures as low as 325 K, and the time-dependent evolution of the magnetization of the ensembles can be imaged in a facile manner, opening up additional avenues for the exploration of thermodynamics of artificial spin ice systems at and above room temperature.

[1] J. S. Gardner, M. J. P. Gingras, and J. E. Greedan, Magnetic pyrochlore oxides, Rev. Mod. Phys. **82**, 53 (2010).

[2] S. T. Bramwell and M. J. P. Gingras, Spin ice state in frustrated magnetic pyrochlore materials, Science **294**, 1495 (2001).

[3] L. J. Heyderman and R. L. Stamps, Artificial ferroic systems: Novel functionality from structure, interactions and dynamics, J. Phys.: Condens. Matter **25**, 363201 (2013).

[4] R. F. Wang, C. Nisoli, R. S. Freitas, J. Li, W. McConville, B. J. Cooley, M. S. Lund, N. Samarth, C. Leighton, V. H. Crespi *et al.*, Artificial 'spin ice' in a geometrically frustrated lattice of nanoscale ferromagnetic islands, Nature (London) **439**, 303 (2006).

[5] C. Nisoli, R. Moessner, and P. Schiffer, *Colloquium*: Artificial spin ice: Designing and imaging magnetic frustration, Rev. Mod. Phys. **85**, 1473 (2013).

[6] S. Ladak, D. E. Read, G. K. Perkins, L. F. Cohen, and W. R. Branford, Direct observation of magnetic monopole defects in an artificial spin-ice system, Nat. Phys. **6**, 359 (2010).

[7] Y. Qi, T. Brintlinger, and J. Cumings, Direct observation of the ice rule in an artificial kagome spin ice, Phys. Rev. B **77**, 094418 (2008).

[8] C. Nisoli, J. Li, X. Ke, D. Garand, P. Schiffer, and V. H. Crespi, Effective Temperature in an Interacting Vertex System: Theory and Experiment on Artificial Spin Ice, Phys. Rev. Lett. **105**, 047205 (2010).

[9] J. P. Morgan, J. Akerman, A. Stein, C. Phatak, R. M. L. Evans, S. Langridge, and C. H. Marrows, Real and effective thermal equilibrium in artificial square spin ices, Phys. Rev. B **87**, 024405 (2013).

[10] J. P. Morgan, A. Stein, S. Langridge, and C. H. Marrows, Thermal ground-state ordering and elementary excitations in artificial magnetic square ice, Nat. Phys. **7**, 75 (2011).

[11] A. Farhan, P. M. Derlet, A. Kleibert, A. Balan, R. V. Chopdekar, M. Wyss, L. Anghinolfi, F. Nolting, and L. J. Heyderman, Exploring hyper-cubic energy landscapes in thermally active finite artificial spin-ice systems, Nat. Phys. **9**, 375 (2013).

[12] V. Kapaklis, U. B. Arnalds, A. Harman-Clarke, E. T. Papaioannou, M. Karimipour, P. Korelis, A. Taroni, P. C. W. Holdsworth, S. T. Bramwell, and B. Hjörvarsson, Melting artificial spin ice, New J. Phys. **14**, 035009 (2012).

[13] U. B. Arnalds, A. Farhan, R. V. Chopdekar, V. Kapaklis, A. Balan, E. T. Papaioannou, M. Ahlberg, F. Nolting, L. J. Heyderman, and B. Hjörvarsson, Thermalized ground state of artificial kagome spin ice building blocks, Appl. Phys. Lett. **101**, 112404 (2012).

[14] S. Zhang, I. Gilbert, C. Nisoli, G.-W. Chern, M. J. Erickson, L. O'Brien, C. Leighton, P. E. Lammert, V. H. Crespi, and P. Schiffer, Crystallites of magnetic charges in artificial spin ice, Nature (London) **500**, 553 (2013).

[15] J. Drisko, S. Daunheimer, and J. Cumings, FePd$_3$ as a material for studying thermally active artificial spin ice systems, Phys. Rev. B **91**, 224406 (2015).

[16] B. Canals, I.-A. Chioar, V.-D. Nguyen, M. Hehn, D. Lacour, F. Montaigne, A. Locatelli, T. O. Menteş, B. S. Burgos, and N. Rougemaille, Fragmentation of magnetism in artificial kagome dipolar spin ice, Nat. Commun. **7**, 11446 (2016).

[17] J. Mizusaki, N. Mori, H. Takai, Y. Yonemura, H. Minamiue, H. Tagawa, M. Dokiya, H. Inaba, K. Naraya, T. Sasamoto *et al.*, Oxygen nonstoichiometry and defect equilibrium in the perovskite-type oxides $La_{1-x}Sr_xMnO_{3+d}$, Solid State Ionics **129**, 163 (2000).

[18] Y. Takamura, R. V. Chopdekar, A. Scholl, A. Doran, J. A. Liddle, B. Harteneck, and Y. Suzuki, Tuning magnetic domain structure in nanoscale $La_{0.7}Sr_{0.3}MnO_3$ islands, Nano Lett. **6**, 1287 (2006).

[19] E. Folven, T. Tybell, A. Scholl, A. Young, S. T. Retterer, Y. Takamura, and J. K. Grepstad, Antiferromagnetic domain reconfiguration in embedded LaFeO$_3$ thin film nanostructures, Nano Lett. **10**, 4578 (2010).

[20] See Supplemental Material at http://link.aps.org/supplemental/10.1103/PhysRevMaterials.1.024401 for transport data, MFM data, and additional X-PEEM images.

[21] Y. Tokura and Y. Tomioka, Colossal magnetoresistive manganites, J. Magn. Magn. Mater. **200**, 1 (1999).

[22] M. S. Lee, T. A. Wynn, E. Folven, R. V. Chopdekar, A. Scholl, A. T. Young, S. T. Retterer, J. K. Grepstad, and Y. Takamura, Tailoring spin textures in complex oxide micromagnets, ACS Nano **10**, 8545 (2016).

[23] K. Steenbeck and R. Hiergeist, Magnetic anisotropy of ferromagnetic $La_{0.7}(Sr,Ca)_{0.3}MnO_3$ epitaxial films, Appl. Phys. Lett. **75**, 1778 (1999).

[24] E. Mengotti, L. J. Heyderman, A. Fraile Rodríguez, A. Bisig, L. Le Guyader, F. Nolting, and H. B. Braun, Building blocks of an artificial kagome spin ice: Photoemission electron microscopy of arrays of ferromagnetic islands, Phys. Rev. B **78**, 144402 (2008).

[25] A. Doran, M. Church, T. Miller, G. Morrison, A. T. Young, and A. Scholl, Cryogenic PEEM at the advanced light source, J. Electron Spectrosc. Relat. Phenom. **185**, 340 (2012).

[26] A. Scholl, H. Ohldag, F. Nolting, J. Stöhr, and H. A. Padmore, X-ray photoemission electron microscopy, a tool for the investigation of complex magnetic structures, Rev. Sci. Instrum. **73**, 1362 (2002).